Published in final edited form as:
Neuron. 2009 November 25; 64(4): 463–470. doi:10.1016/j.neuron.2009.10.015.

Classical MHCI molecules regulate retinogeniculate refinement and limit ocular dominance plasticity

Akash Datwani[1,2], **Michael J. McConnell**[1,3], **Patrick O. Kanold**[4], **Kristina D. Micheva**[5], **Brad Busse**[5], **Mehrdad Shamloo**[6], **Stephen J. Smith**[5], and **Carla J. Shatz**[1]

[1]Departments of Biology, Neurobiology & Bio-X, James H. Clark Center, 318 Campus Drive W1.1, Stanford University, Stanford, CA 94305-5437 USA

[5]Departments of Molecular and Cellular Physiology, Stanford University School of Medicine, Stanford, CA 94305 USA

[6]Behavioral and Functional Neuroscience Laboratory, Institute of Neuro-Innovation and Translational Neurosciences, Stanford University, Stanford, CA 94305 USA

Abstract

Major histocompatibility complex Class I (MHCI) genes were discovered unexpectedly in healthy CNS neurons in a screen for genes regulated by neural activity. In mice lacking just 2 of the 50+ MHCI genes H2-K^b and H2-D^b, ocular dominance (OD) plasticity is enhanced. Mice lacking PirB, an MHCI receptor, have a similar phenotype. H2-K^b and H2-D^b are expressed not only in visual cortex, but also in lateral geniculate nucleus (LGN) where protein localization correlates strongly with synaptic markers and complement protein C1q. In $K^bD^{b-/-}$ mice developmental refinement of retinogeniculate projections is impaired, similar to C1q-/- mice. These phenotypes in $K^bD^{b-/-}$ mice are strikingly similar to those in $\beta2m^{-/-}TAP1^{-/-}$ mice, which lack cell surface expression of all MHCIs, implying that H2-K^b and H2-D^b can account for observed changes in synapse plasticity. H2-K^b and H2-D^b ligands, signaling via neuronal MHCI receptors, may enable activity-dependent remodeling of brain circuits during developmental critical periods.

INTRODUCTION

Brain circuits are refined by early spontaneous activity and later on by sensory experience (Katz and Shatz, 1996; Knudsen, 2004). In the developing mammalian visual system, spontaneous activity generated in retinal ganglion cells (RGCs) and relayed to the lateral geniculate nucleus (LGN) drive initially intermixed retinogeniculate connections to refine into non-overlapping eye-specific layers; blockade or perturbation of waves prevents refinement (Huberman et al., 2008; Stellwagen and Shatz, 2002). How neural activity ultimately leads to

Corresponding author: Carla J. Shatz, James H. Clark Center, 318 Campus Drive, W 1.1 Room W157, Stanford University Stanford, CA 94305-5437, TEL: 650-723-0534, FAX: 650-723-4442, cshatz@stanford.edu.
[2]Current address: Elan Pharmaceuticals Inc., South San Francisco, CA 94080 USA
[3]Current address: Crick-Jacobs Center for Theoretical and Computational Biology, Salk Institute for Biological Studies, La Jolla, CA 92037 USA
[4]Current address: Department of Biology, 1116 Biosciences Res. Bldg., University of Maryland, College Park, MD 20742 USA

COMPETING INTEREST STATEMENT The authors declare no competing financial interests.

refinement is not well understood, but it is known that synapse elimination, as well as synapse strengthening and stabilization, are involved (Butts et al., 2007; Chen and Regehr, 2000; Hooks and Chen, 2006; Mooney et al., 1993).

To discover genes downstream of spontaneous retinal activity, we conducted an unbiased screen in which activity was blocked by tetrodotoxin (TTX) during the period of eye-specific segregation (Corriveau et al., 1998). TTX not only prevents retinogeniculate refinement (Shatz and Stryker, 1988; Sretavan et al., 1988), but unexpectedly also downregulated the expression of MHC Class I mRNA in neurons. MHCI (Major Histocompatibility Class I), a large and highly polymorphic family of 50+ genes, some with well known roles in the immune system and T-cell function (Zinkernagel and Doherty, 1979), were not previously thought to be expressed by neurons in the healthy brain, let alone regulated by neural activity.

Here, by examining mice lacking both H2-K^b and H2-D^b (Histocompatibility Locus 2; Schott et al., 2003), we show that these 2 genes are required for retinogeniculate refinement. In the immune system H2-K^b and H2-D^b bind and signal not only via the T-cell receptor, but also via PirB (Paired immunoglobulin-like receptor B), an innate immune receptor (Takai, 2005) also expressed in visual cortical neurons (Syken et al, 2006). We report that $K^bD^{b-/-}$ mice have enhanced ocular dominance (OD) plasticity, similar to PirB mutant mice (Syken et al., 2006). These findings imply a novel role for these 2 specific MHCI molecules and cognate immune receptors in activity-dependent plasticity during CNS development. Given the recent association between human Histocompatibility Locus (HLA) and Schizophrenia (Purcell et al., 2009; Shi et al., 2009; Stefansson et al., 2009), our findings also reveal a novel way to explore potential links between immune and nervous systems: via the disruption of normal MHCI regulation of plasticity at neuronal synapses.

RESULTS

Enhanced ocular dominance plasticity in $K^bD^{b-/-}$ mice

In the immune system, H2-K^b and H2-D^b bind and signal via a variety of receptors, including PirB (Nakamura et al., 2004; Takai, 2005). Cortical neurons not only express PirB, but also mice lacking PirB have enhanced OD plasticity following monocular deprivation or eye removal (Syken et al., 2006). Because cortical neurons express both H2-K^b and H2-D^b (Huh et al, 2000; Figure S1), we examined if OD plasticity is also perturbed in $K^bD^{b-/-}$ mutant mice. To create a large imbalance in visually driven inputs to neurons normally receiving binocular inputs, one eye was deprived (MD) or enucleated (ME) at P22, just at the onset of the critical period in visual cortex but after eye segregation in the LGN is adult-like (Frenkel and Bear, 2004; Rossi et al., 2001; Tagawa et al., 2005).

The spatial extent of input from the eyes to visual cortex was assessed functionally at P31 by in situ hybridization for the immediate early gene Arc. After a 30-minute monocular light exposure, Arc mRNA is upregulated (induced) rapidly (Syken et al., 2006; Tagawa et al., 2005) in visually stimulated cortical neurons (Figure 1A). Following ME or MD, this method reports OD plasticity reliably, as measured by the pronounced expansion in width of Arc mRNA signal in visual cortex ipsilateral to the stimulated (open) eye (Syken et al., 2006; Tagawa et al., 2005). This expansion in width of Arc induction correlates with the well-known strengthening of the open eye following monocular deprivation assessed in physiological studies measuring single units (Antonini et al., 1999), visually-evoked potentials (VEPs) (Frenkel and Bear, 2004; Iny et al., 2006) or optical imaging (Cang et al., 2005; Hubener, 2003) and faithfully detects OD plasticity with the advantage here of laminar and cellular resolution. As expected (Tagawa et al., 2005), ME in wildtype mice (WT: $K^bD^{b+/+}$) led to a 51% increase in width of Arc induction in layer 4 of visual cortex ipsilateral to the remaining eye, as compared to normally reared WT mice (Figure 1C).

By contrast, Arc induction in $K^bD^{b-/-}$ mice following ME is *even wider*; indicating that OD plasticity following ME is greater in $K^bD^{b-/-}$ than WT mice. However, in $K^bD^{b-/-}$ mice reared with normal vision, the width of Arc induction ipsilateral to the stimulated eye is already about 22% greater than WT (cf. Figure 1B,C). This initially expanded ipsilateral representation might account entirely for the greater OD plasticity observed in $K^bD^{b-/-}$ mice. Thus, to compare the extent of OD plasticity between the different genotypes, we computed a "plasticity index" (=width of Arc induction following ME/width following normal visual rearing; Figure 1D) that factors in the different starting points for each genotype. The plasticity index for $K^bD^{b-/-}$ (2.16 ± 0.11) is 65% larger than for WT (1.51 ± 0.08, Figure 1D), indicating that even after correcting for the expanded representation of the ipsilateral eye in normally reared $K^bD^{b-/-}$ mice, OD plasticity is significantly enhanced.

To exclude the possibility that enhanced OD plasticity after eye removal in $K^bD^{b-/-}$ mice is due to an injury response, rather than visual deprivation, experiments were repeated using MD at similar ages (Figure 1C). A more modest expansion in width of Arc induction was detected than after ME (Tagawa et al., 2005). Nevertheless following MD, the width of Arc signal in $K^bD^{b-/-}$ mice, as well as the plasticity index, is 17% greater than that in WT mice (plasticity index: 1.48 ± 0.103 $K^bD^{b-/-}$; 1.31 ± 0.105 $K^bD^{b+/+}$; $P = 0.042$; Figure 1C, D). These differences in OD plasticity in $K^bD^{b-/-}$ vs. WT mice are also not likely due to differences in visual ability. We examined this possibility behaviorally in normally reared mice using a visual acuity water maze test (Prusky et al., 2000; Robinson et al., 2001). Acuity is similar in WT and $K^bD^{b-/-}$ mice (Figure S2: A-F), suggesting that the expanded representation of the ipsilateral eye within the BZ of visual cortex following MD or ME is not from degraded vision in the mutant mice. Indeed, following ME in mutant mice, visual acuity is, if anything, slightly better than in WT mice (Figure S2: G-I), possibly reflecting a behavioral consequence of enhanced OD plasticity. Thus, like PirB (Syken et al., 2006), H2-K^b and/ or H2-D^b appear to limit the extent of OD plasticity following MD or ME during the critical period.

The vast majority of MHCI cell surface proteins can be abrogated by genetically deleting β2m, a subunit needed for MHCIs, and/or the peptide loading-associated molecule TAP1 (Ljunggren et al., 1995; Zinkernagel and Doherty, 1979). In the brains of $\beta2m^{-/-}$, or $\beta2m^{-/-}TAP1^{-/-}$ mice, there are changes in hippocampal synaptic plasticity, homeostatic scaling (Goddard et al., 2007; Huh et al., 2000), motor learning (McConnell et al., 2009), pheromone driven behavior (Loconto et al, 2003), and motoneuron axon regeneration (Oliveira et al., 2004). In addition, following ME here, the width of Arc induction in visual cortex of $\beta2m^{-/-}$ and $\beta2m^{-/-}TAP1^{-/-}$ mice is similar to that in $K^bD^{b-/-}$ mice (Figure 1C, 1D, and data not shown: $\beta2m^{-/-}TAP^{-/-}$+ME: 2258.8 ± 120.2 μm, $n = 38$ mice, $P = 0.0032$; $K^bD^{b-/-}$+ME: 2404.6 ± 105.1 μm, $n = 25$ mice, $P = 0.0017$) The plasticity index is also 44% greater than for WT ($\beta2m^{-/-}TAP^{-/-}$ = 2.08 ± 0.140; $\beta2m^{+/+}TAP1^{+/+}$ = 1.64 ± 0.080; $P = 0.0078$), similar to that for $K^bD^{b-/-}$ mice (2.16 ± 0.11). These observations suggest that loss of just H2-K^b and H2-D^b can account for enhanced OD plasticity seen in visual cortex of mice lacking surface expression of the majority of MHCI proteins.

Expanded thalamocortical projections to layer 4 of $K^bD^{b-/-}$ mice following ME

The expansion of Arc signal in layer 4 following ME or MD could arise from at least two non-mutually exclusive possibilities: (1) thalamocortical axons could have a wider distribution and therefore contact more neurons in layer 4; and/or (2) the expansion in Arc signal could result from changes in intracortical connections. To explore these possibilities, transneuronal tracing, using ^{3}H-proline (Antonini et al., 1999; LeVay et al., 1978; Syken et al., 2006) was performed after ME in WT (n = 5) or $K^bD^{b-/-}$ (n = 7) mice. Similar to Arc induction, transneuronal tracing labels a wider patch in $K^bD^{b-/-}$ than in WT mice (Figure 2B, C). Even so, the width measured from transneuronal transport is about 70% smaller than that from Arc induction (cf. Figure.

1C, 2C), suggesting that expansion of thalamocortical axons alone cannot account entirely for the increased OD plasticity observed in $K^bD^{b-/-}$mice; changes in intracortical connections likely also contribute.

Abnormal retinogeniculate patterning in $K^bD^{b-/-}$ mice

Blockade of neural activity prevents developmental refinement of retinogeniculate projections (Huberman et al., 2008) and down-regulates MHCI mRNA and protein (Corriveau et al., 1998; Goddard et al., 2007). $K^bD^{b-/-}$ mutant mice resemble the situation in which 2 MHCI molecules have been completely down-regulated by activity blockade. To examine if H2-K^b and H2-D^b could be involved in refinement of the retinogeniculate projection, we first assessed expression in the dLGN by immunostaining (Figure S1C). Protein can be detected in LGN neurons at P9, during the period of activity-dependent refinement of the retinogeniculate projection. Expression has decreased by P34, after refinement is complete, consistent with transient expression of MHCI mRNA in the LGN (Huh et al, 2000).

To assess the distribution of retinal ganglion cell (RGC) terminals, we made intraocular injections of different fluorophores into the each eye (Experimental Procedures, (Torborg and Feller, 2004). The LGN territory occupied by RGC projections was assessed at P34, 3 weeks after projections normally have completely segregated (Figure 3A, Figure S3). The percent LGN area occupied by projections from the ipsilateral eye in $K^bD^{b-/-}$ mice (24.99 ± 2.97%) is almost twice that of WT (12.75 ± 2.42%, Figure 3B), while total LGN area is similar between genotypes.

Abnormal segregation of eye-specific inputs in dLGN of $K^bD^{b-/-}$

An increase in area of the ipsilateral eye projection to the LGN could come at the cost of contralateral eye territory, or if RGC inputs failed to segregate (Torborg and Feller, 2004). Using fluorescent double labeling to examine projections from both eyes simultaneously at P34, significantly increased overlap of RGC projections from the two eyes was observed in $K^bD^{b-/-}$ vs. WT mice (Figure 3; for both hemispheres see Figure S3B). These changes in the retinogeniculate projection of $K^bD^{b-/-}$ mice also almost exactly phenocopy $\beta2m^{-/-}TAP1^{-/-}$ mice (Figure S3B; Huh et al., 2000). Using multiple threshold analysis (Experimental procedures (Torborg and Feller, 2004), we find that overlap of RGC inputs, measured by pixels common to both red and green channels, is significantly greater in all MHCI mutant mouse lines over WT controls (Figure S3C, D). For example, at 60% maximal threshold, the percent of dLGN area with overlapping pixels is 19.10 ± 2.80% in $K^bD^{b-/-}$; 15.50 ± 3.01% in $\beta2m^{-/-}TAP1^{-/-}$; but only 4.23 1.77% in WT (Figure S3D). On average across examined intensity thresholds there is approximately a 3 – 5 fold increase in overlap in mutant mice over WT (Figure S3D). These findings suggest that normal retinogeniculate refinement may require just H2-K^b and H2-D^b.

Given the enhanced OD plasticity noted in visual cortex of mutant mice, we wondered if RGC projections in mutant mice remain stable even after retinogeniculate segregation is normally completed. If not, ME might cause further expansion of the RGC projection within the LGN. Intraocular injections of CTB-AF488 were performed to label retinal afferents subsequent to ME between P22-31 in WT (n = 6) and $K^bD^{b-/-}$ (n = 6) mice and the percent LGN area occupied by the ipsilateral RGC projection was measured. There was no change observed in either genotype, the developmentally-expanded ipsilateral eye inputs remained stable. This observation correlates with our finding that the expression of both H2-K^b and H2-D^b is developmentally downregulated by P34, and demonstrates that the enhanced OD plasticity seen in visual cortex of mutant mice during the critical period is not due to a reorganization of RGC projections following ME.

MHCI Immunostaining is associated with LGN synapses and C1q

A direct role for H2-K^b and/or H2-D^b in refinement of RGC projections would be supported by synaptic localization of these proteins. To determine if MHCI localizes near synapses in vivo, Array Tomography (AT) (Micheva and Smith, 2007) was used to examine immunostained LGN sections at P7, at time when eye-specific layer formation is in progress and LGN expression levels of C1q (Stevens et al, 2007) and MHCI (Figure S1; Huh et al, 2000) are high. This method permits immunostaining of the same ultrathin 70nm section repeatedly for known synaptic markers, as well as for MHCI and other molecules of interest (Figure 4A). Serial sections are then tomographically reassembled, rendering a 3-dimensional image containing patterns of protein localization. In AT images, MHCI is localized in a punctate pattern, often closely associated both with PSD-95 and/ or synapsin puncta (Figure 4A), consistent with previous observations of hippocampal neurons in vitro (Goddard et al., 2007).

Higher resolution examination of 4 serial sections (Figure 4B) shows MHCI puncta associated with excitatory and inhibitory synapses, as well as with C1q, a complement protein recently also found to be required for RGC refinement and synapse elimination (Stevens et al., 2007). To assess these relationships quantitatively, a cross-correlation pixel analysis was performed (Figure 4C, D and Figure S4 online; Experimental procedures). As expected, pre- (synapsin I) and post- (postsynaptic density-95) synaptic markers are highly correlated with each other, while inhibitory (GAD) and excitatory (vGluT2) markers are not correlated with each other since they are not associated with similar synaptic types. Close association of MHCI molecules and C1q at synapses is consistent with the observation here that the specific MHCI molecules H2-K^b and H2-D^b, like C1q, are needed for retinogeniculate synapse refinement.

DISCUSSION

In mice lacking expression H2-K^b and H2-D^b, retinal projections to the LGN fail to refine completely, and within visual cortex, OD plasticity is enhanced. These changes phenocopy those present in $\beta2m^{-/-}TAP1^{-/-}$ mice, which lack stable cell-surface expression of most of the 50+ MHCIs (Ljunggren et al., 1995). Because H2-K^b and H2-D^b mRNA and protein are present in neurons within LGN and visual cortex, we propose that these specific classical MHCI family members are not only required for activity-dependent refinement and plasticity in the visual system, but can account for the majority of the abnormalities observed in the visual system of $\beta2m^{-/-}TAP1^{-/-}$ mice.

MHCI function during developmental refinement of the retinogeniculate projection

Many experiments have shown that when neural activity is blocked or altered, segregation of RGC afferents from the two eyes within the dLGN is incomplete (Penn et al., 1998; Stellwagen and Shatz, 2002). Here we show that H2-D^b and H2-K^b are expressed in the dLGN primarily during the period of eye-specific segregation and that, in their absence, RGC afferents fail to segregate fully. The Array Tomography data provides strong support for the proposal that these MHCI proteins are located near or at synapses, but the resolution of the method is still not sufficient to conclude that they are situated at the pre- or the postsynaptic membrane. Here, we found a higher correlation between MHCI and PSD-95 than between MHCI and synapsin, consistent with previous observations of immunostaining associated with neuronal dendrites in vivo (Corriveau et al, 1998; McConnell et al, 2009), as well as with synapses and PDS-95 in vitro (Goddard et al, 2007). Together, these observations place MHCI at the postsynaptic membrane, but this suggestion must await electron microscopy, fix-insensitive MHCI antibodies and or biochemical fractionation for confirmation.

The failure of RGC axons from the two eyes to segregate completely from each other even in the presence of intact retinal wave activity (Huh et al, 2000) implies H2-K^b and/or H2-D^b may function as molecular read-outs for activity-dependent synapse weakening and elimination. Other immune system molecules have also been implicated in retinogeniculate synapse elimination. Like MHCI, neuronal pentraxins (e.g., NP1 and NP2), proteins homologous to immune system pentraxins, are upregulated by neuronal activity (Bjartmar et al., 2006). In addition, the complement proteins C1q and C3 are present in the dLGN during retinogeniculate refinement (Stevens et al., 2007). $NP1^{-/-}NP2^{-/-}$ as well as $C1q^{-/-}$ and $C3^{-/-}$ mutant mice have dLGN phenotypes strikingly similar to those reported here. The localization of MHCI and C1q is highly correlated, implying that these two molecules could interact and function together in developmental remodeling at excitatory as well as inhibitory synapses. Note that PirB cannot be detected in the LGN during the period of retinogeniculate remodeling (Syken et al, 2006), but CD3ζ, a signaling component for other immune receptors, is present. CD3ζ mutant mice also have defects in retinogeniculate refinement (Huh et al, 2000), implying that H2-D^b and H2-K^b in the LGN may collaborate with a CD3ζ–containing receptor.

The phenotypes observed in complement-deficient and in MHCI mutant mice are stable and persist into adulthood. In contrast, the defect in $NP1^{-/-}NP2^{-/-}$ is transient (Bjartmar et al., 2006). Thus it may be that a series of tightly developmentally regulated events operate sequentially to establish connectivity, then to stabilize and cluster glutamate receptors (a process involving neuronal pentraxins; Bjartmar et al., 2006) and finally to remodel and eliminate synaptic inputs in an MHCI-C1q activity-dependent manner. The precise mechanisms of how synapses are tagged for elimination based on their activity is far from understood, but MHCI appears well-suited to act in this process, given that action potential blockade downregulates both mRNA and protein (Corriveau et al., 1998; Goddard et al., 2007).

H2-K^b and H2-D^b may function with PirB to limit OD Plasticity in Visual Cortex

The presence of enhanced OD plasticity in the visual cortex of mutant mice studied here is notable. First, it argues for a role for H2-K^b and H2-D^b in limiting the extent of strengthening of the open (remaining) eye following an imbalance in activity created by eye removal or closure. Just how the open eye is able to gain so much functional territory in the visual cortex of $K^bD^{b-/}$ mice following visual deprivation remains to be fully explored. Following ME in the mutant mice, we have shown that there is a large mismatch in extent of expansion of the ipsilateral thalamocortical projection as assessed using transneuronal tracing compared with that assessed using induction of Arc mRNA. The expansion, as measured from anatomical tracing, is far less than that measured functionally from the response of cortical neurons to visual stimulation, suggesting that the enhanced OD plasticity in $K^bD^{b-/}$ mice may reflect not only the presence of a larger pool of ipsilateral geniculocortical axons, but also changes within the cortex. Future experiments will be required to elucidate how loss of these 2 MHCI family members alters the details of connectivity, as well as rules of synaptic plasticity, at the cellular level.

H2-K^b and H2-D^b join a very limited number of other molecules whose *loss* of function also results in *enhanced*, rather than diminished, OD plasticity. This small group includes Nogo signaling ($NgR^{-/-}$, $NogoA/B^{-/-}$ mice; (McGee et al., 2005) and PirB (Syken et al., 2006), as well as infusion of tPA (Mataga et al., 2002) which alters the extracellular matrix in cortex. PirB is expressed on certain cells of the innate immune system and is a known receptor for H2-K^b and H2-D^b (Nakamura et al., 2004). PirB is expressed in subsets of neurons including many pyramidal neurons of the cerebral cortex (but notably is not detected in LGN neurons) and PirB has recently been shown to bind Nogo (Atwal et al., 2008). Mice lacking PirB have enhanced OD plasticity (Syken et al., 2006) almost identical to that seen here in $K^bD^{b-/}$ mice. Together

these observations suggest that PirB functions as a neuronal receptor for H2-K^b and H2-D^b, possibly even in collaboration with NgR/Nogo. In cultured cortical neurons, PirB immunostaining is associated with axonal growth cones and is located near synapses (Syken et al., 2006), while MHCI immunostaining is present in neuronal dendrites and colocalizes with PSD-95 (Goddard et al., 2007), implying a model in which postsynaptic MHCI interacts across the synapse with presynaptic PirB (Shatz, 2009). Thus, MHCI-PirB signaling may operate either in parallel or in conjunction with these other molecules to regulate negatively the strength and stability of synaptic connections in an activity-dependent manner.

EXPERIMENTAL PROCEDURES

Animals and Genotyping of mouse lines

The Institutional Animal Care and Use Committees at Harvard Medical School and Stanford University approved all protocols. Animals were raised in a pathogen-free facility, all mutant mice were outwardly normal. $\beta2m^{-/-}TAP1^{-/-}$ mice were obtained from D. Raulet (Dorfman et al., 1997). Widltype ($\beta2m^{+/+}TAP1^{+/+}$) and singly mutant mice were derived by backcrossing $\beta2m^{-/-}TAP1^{-/-}$ to the same background strain of C57BL/6 wildtype mice purchased from Charles River (Wilmington, MA) for more than five generations to obtain mice carrying the wildtype alleles for both β2m and TAP1 genes. To avoid genetic drift, homozygous parents in each of these four colonies are obtained from a common breeding colony containing mixed heterozygote genotypes. Genotyping of β2m and TAP1 alleles was performed by PCR as described previously (Huh et al., 2000). $K^bD^{b-/-}$ mice on a C57BL/6 genetic background were obtained from H. Ploegh (Schott et al., 2003) and maintained as a homozygous breeding colony. Age-matched C57BL/6 controls were purchased from Charles River (Wilmington, MA).

Mouse surgery and OD plasticity experiments

For monocular enucleation (ME) experiments to assess OD plasticity mice were anesthetized at P22 with isofluorane, one eye was removed (if needed sterile gelfoam was inserted in the orbit to minimize bleeding). Eyelids were trimmed and sutured with 6-0 sterile surgical silk. A drop of Vetbond (3M, St. Paul, MN) was put on sutured eyelids to prevent reopening. For monocular deprivation (MD) experiments, mice were anesthetized at P25 and the procedure was identical as described above except the eye was not removed until the day prior to Arc induction.

Arc induction

At P31 (for ME) or at P34 (for MD) one eye was removed under anesthesia (unless ME had already been performed at an earlier age, as in OD plasticity experiments); mice were revived and put in total darkness for 8 - 12 hours to minimize basal levels of Arc mRNA in visual cortex. Mice were returned to a lighted environment for 30 minutes to induce Arc mRNA in the cortex driven by vision through the remaining eye. After light exposure, mice were euthanized with Halothane (Halocarbon, River Edge NJ), brains were removed, flash-frozen in M-1 embedding media (Thermo Scientific, Waltham, MA) and 14μm thick coronal sections were processed for situ hybridization with Arc antisense riboprobe (Syken et al., 2006; Tagawa et al., 2005). Arc plasmid was provided by Dr. P. Worley, Johns Hopkins University, Baltimore, MD.

Densitometric scans of Arc induction in specific cortical layers

Quantitative analysis of Arc induction by stimulation of the ipsilateral eye was performed in MATLAB (Mathworks, Inc, Natick, MA) by line scans across layer 4 of primary and secondary visual cortex (Figure 5B) as described previously (Tagawa et al., 2005): for each animal the width of Arc mRNA signal two standard deviations above background was measured in 3 - 4

sections scanned in randomized order, blind to genotype and manipulation. Slides from different animals and manipulations were interleaved and only reassembled once all width measurements were computed. Between 7-28 animals of each genotype were studied; average widths of Arc induction were computed for each animal and displayed in cumulative histograms (Figure 1B).

Transneuronal labeling

To visualize the pattern of geniculocortical projections to layer 4 of mouse visual cortex 1-2 μl of L-[2,3,4,5-3H]-proline (GE Healthcare, Cat#TRK750; approx. 100 Ci/mmol) was injected intraocularly at a concentration of 150-200μCi/μl dissolved in 0.1M PBS pH 7.4; a week later mice were euthanized with euthasol 50mg/kg, brains were frozen in M-1 mounting medium (ThermoShandon) and 14 μm coronal cryosections were prepared on glass superfrost *Plus* slides (Fisher scientific). Sections were fixed in 4% paraformaldehyde in PBS, pH 7.4, washed twice in 0.1M PBS and dehydrated through a graded ethanol series. Sections were coated with NTB-2 emulsion (Kodak, Inc.), dried in dark room, and then stored at 4°C. After 2-3 months, slides were developed and imaged using dark field microscopy. Width measurements of transported radioactive signal were measured in MATLAB (Mathworks, Inc) by making line scans across layer 4 of primary and secondary visual cortex, as described for Arc in situ measurements above and as used previously (Tagawa et al., 2005).

Anterograde labeling of retinal ganglion axons and multiple threshold analysis

P31-34 mice were anesthetized with isofluorane (in the case of LGN plasticity experiments ME was performed from P22-31) then 1 - 2μl of cholera toxin B (CTB) subunit conjugated to AF488 was injected in the right eye and AF594 in the left (1mg/mL dissolved in 0.2% DMSO in nuclease-free water; Invitrogen, Inc. Carlsbad, CA). After 24 hours, animals were overdosed with euthasol (50mg/kg), brains fixed by transcardial perfusion of 0.1M PBS then ice-cold 4% PFA in 0.1M PBS. Brains were removed, postfixed overnight in 4% PFA in 0.1M PBS at 4° C, then sectioned coronally using a vibratome at 100μm. Sections were mounted with prolong antifade gold media (Invitrogen, Inc. Carlsbad, CA) on glass sides, and coverslipped for imaging on a Zeiss LSM 510 META confocal microscope (Carl Zeiss MicroImaging, Inc. Thornwood, NY)

All analysis was performed blind to genotype. To minimize variability analysis was performed on dLGN sections where the ipsilateral projection area was the largest, typically at the middle of the rostral-caudal extent of the dLGN (Figure S3B online). All images were acquired such that the peak intensity values were just below saturating and multiple threshold analysis was carried out for the series of signal thresholds, described previously (Torborg and Feller, 2004). In brief, dLGN sections were imaged in the red and then green channel, and by varying each ipsi and contra channel at each intensity threshold of 20%, 40%, 60%, 80% and 100% of maximum. To obtain overlap measurements, the amount of overlapping red and green pixels in LGNs in both hemispheres was measured in Image J (NIH, Bethesda, MD) using the Colocalization plugin tool and displayed as yellow pixels (Figure 3A lower panel, overlap). The total area of overlapping pixels was represented as a percentage of total dLGN area (Figure 3C).

Array Tomography

Two postnatal day (P)7 mice, were perfused intracardially with 0.1M PBS, followed by 4% paraformaldehyde in 0.1M PBS and the tissue was processed for array tomography (Micheva and Smith, 2007). The LGN was dissected out, further fixed in the same fixative using microwave irradiation (PELCO 3451 laboratory microwave system; Ted Pella), then dehydrated in ethanol and embedded in LRWhite resin (medium grade, SPI). Serial ultrathin sections (70 nm) were cut on an ultramicrotome (Leica), mounted on subbed coverslips and

immunostained using either of two MHCI antibodies that yielded similar AT staining patterns (Ox18, 1:50 AbDSerotec Cat#MCA51G or ErHr52, 1:10 BMA Cat#T2105). For secondary antibodies, Alexa 488, Alexa 594 and Alexa 647 (Invitrogen, 1:150) from the appropriate species were used. Up to 3 antibodies from different hosts were applied together and imaged, followed by an antibody elution. Sections were then restained with a different set of antibodies and re-imaged. Other antibodies included those against synaptic proteins: synapsin I (rabbit, Millipore AB1543P, 1:100), PSD-95 (mouse, NeuroMabs 75-028, 1:100), GAD65/67 (rabbit, Millipore AB1511, 1:300), vGluT2 (guinea pig, Millipore AB2251, 1:1000), as well as a C1q antibody (goat, Quidel A301, 1:300; ref. 31). Sections were mounted using SlowFade Gold antifade reagent with DAPI (Invitrogen). Imaging was done on a Zeiss AxioImager.Z1 fluorescence microscope with AxioCam HRm CCD camera, using a Zeiss 63x/1.4 NA Plan Apochromat objective. Images were aligned using ImageJ and the Multistack Reg plugin.

Array Tomography Cross-Correlation Analysis of synaptic markers, MHCI, and C1q

To examine the spatial relationship between known synaptic markers and MHCI and C1q, we used a cross-correlation analysis method similar to that described previously (van Steensel et al., 1996). For each pair of channels analyzed, a cross-correlation score Si was computed over a range of lateral offset distances for images in the two channels. Differences in the mean brightness in different channels were corrected by repeating the analysis with one channel transposed (and therefore uncorrelated) to obtain a baseline score St. To ensure that only labeled molecules in the synaptic neuropil were included, the DAPI channel was used as a mask to remove nuclear and somatic staining from the analysis. Si/St = Cr, describing the correlation (Cr) between two channels as a multiple of their baseline correlation. A Cr of 1 indicates no correlation, Cr $\gg$ 1 indicates high correlation, and Cr < 1 indicates negative correlation. This method of analysis enables one to directly compare the correlation of different immunolabels in a channel-independent manner (Figure 4D).

Statistical analyses

Statistical comparisons were performed using Excel (Microsoft Corp., Redmond, WA). Tests on independent groups were Mann Whitney *U* test for comparisons of cumulative distributions (widths of Arc mRNA signal or radioactively labeled thalamocortical terminals in layer 4) with population samples of unequal size, two-tailed Student's *t* test for group comparisons of LGN areas, two-way ANOVA for LGN pixel overlap across multiple thresholds, and one-way ANOVA for Plasticity Index comparisons.

Supplementary Material

Refer to Web version on PubMed Central for supplementary material.

Acknowledgments

We thank members of the Shatz lab for helpful suggestions and comments. For technical assistance we thank B. Printseva, M. Marcotrigiano, J. Neville-Golden, and P. Kemper. $\beta 2m^{-/-}$-$TAP1^{-/-}$ mice were a gift from D. Raulet (UC Berkeley, Berkeley CA) and $K^bD^{b-/-}$ mice from H. Ploegh (MIT, Cambridge MA). We thank Dr. Beth Stevens (Harvard Medical School, Boston MA) for providing the C1q antibody and helpful discussions on using Array Tomography. Thanks also to Matthew Priestley and Nay Lui Saw of the Stanford Institute for Neuroinnovation and Translational Neuroscience NeuroBehavior Core Facility. This work was supported by NIH R01 EY02858, NIH R01 MH071666, the G. Harold and Leila Y. Mathers Charitable Foundation, the Dana Foundation (CJS & AD), and NIH T32CA09361 (MJM).

References

Antonini A, Fagiolini M, Stryker MP. Anatomical correlates of functional plasticity in mouse visual cortex. J Neurosci 1999;19:4388–4406. [PubMed: 10341241]

Atwal JK, Pinkston-Gosse J, Syken J, Stawicki S, Wu Y, Shatz C, Tessier-Lavigne M. PirB is a functional receptor for myelin inhibitors of axonal regeneration. Science (New York, N Y 2008;322:967–970.

Bjartmar L, Huberman AD, Ullian EM, Renteria RC, Liu X, Xu W, Prezioso J, Susman MW, Stellwagen D, Stokes CC, et al. Neuronal pentraxins mediate synaptic refinement in the developing visual system. J Neurosci 2006;26:6269–6281. [PubMed: 16763034]

Butts DA, Kanold PO, Shatz CJ. A burst-based "Hebbian" learning rule at retinogeniculate synapses links retinal waves to activity-dependent refinement. PLoS biology 2007;5:e61. [PubMed: 17341130]

Cang J, Kalatsky VA, Lowel S, Stryker MP. Optical imaging of the intrinsic signal as a measure of cortical plasticity in the mouse. Visual neuroscience 2005;22:685–691. [PubMed: 16332279]

Chen C, Regehr WG. Developmental remodeling of the retinogeniculate synapse. Neuron 2000;28:955. [PubMed: 11163279]

Corriveau RA, Huh GS, Shatz CJ. Regulation of class I MHC gene expression in the developing and mature CNS by neural activity. Neuron 1998;21:505–520. [PubMed: 9768838]

Dorfman JR, Zerrahn J, Coles MC, Raulet DH. The basis for self-tolerance of natural killer cells in beta2-microglobulin- and TAP-1- mice. J Immunol 1997;159:5219–5225. [PubMed: 9548460]

Frenkel MY, Bear MF. How monocular deprivation shifts ocular dominance in visual cortex of young mice. Neuron 2004;44:917–923. [PubMed: 15603735]

Goddard CA, Butts DA, Shatz CJ. Regulation of CNS synapses by neuronal MHC class I. Proceedings of the National Academy of Sciences of the United States of America 2007;104:6828–6833. [PubMed: 17420446]

Hooks BM, Chen C. Distinct roles for spontaneous and visual activity in remodeling of the retinogeniculate synapse. Neuron 2006;52:281–291. [PubMed: 17046691]

Hubener M. Mouse visual cortex. Current opinion in neurobiology 2003;13:413–420. [PubMed: 12965287]

Huberman AD, Feller MB, Chapman B. Mechanisms Underlying Development of Visual Maps and Receptive Fields. Annual review of neuroscience 2008;31:479–509.

Huh GS, Boulanger LM, Du H, Riquelme PA, Brotz TM, Shatz CJ. Functional requirement for class I MHC in CNS development and plasticity. Science (New York, N Y 2000;290:2155–2159.

Iny K, Heynen AJ, Sklar E, Bear MF. Bidirectional modifications of visual acuity induced by monocular deprivation in juvenile and adult rats. J Neurosci 2006;26:7368–7374. [PubMed: 16837583]

Katz LC, Shatz CJ. Synaptic activity and the construction of cortical circuits. Science (New York, N Y 1996;274:1133–1138.

Knudsen EI. Sensitive periods in the development of the brain and behavior. J Cogn Neurosci 2004;16:1412–1425. [PubMed: 15509387]

LeVay S, Stryker MP, Shatz CJ. Ocular dominance columns and their development in layer IV of the cat's visual cortex: a quantitative study. The Journal of comparative neurology 1978;179:223–244. [PubMed: 8980725]

Ljunggren HG, Van Kaer L, Sabatine MS, Auchincloss H Jr, Tonegawa S, Ploegh HL. MHC class I expression and CD8+ T cell development in TAP1/beta 2-microglobulin double mutant mice. International immunology 1995;7:975–984. [PubMed: 7577806]

Mataga N, Nagai N, Hensch TK. Permissive proteolytic activity for visual cortical plasticity. Proceedings of the National Academy of Sciences of the United States of America 2002;99:7717–7721. [PubMed: 12032349]

McConnell MJ, Huang YH, Datwani A, Shatz CJ. H2-K(b) and H2-D(b) regulate cerebellar long-term depression and limit motor learning. Proceedings of the National Academy of Sciences of the United States of America 2009;106:6784–6789. [PubMed: 19346486]

McGee AW, Yang Y, Fischer QS, Daw NW, Strittmatter SM. Experience-driven plasticity of visual cortex limited by myelin and Nogo receptor. Science (New York, N Y 2005;309:2222–2226.

Micheva KD, Smith SJ. Array tomography: a new tool for imaging the molecular architecture and ultrastructure of neural circuits. Neuron 2007;55:25–36. [PubMed: 17610815]

Mooney R, Madison DV, Shatz CJ. Enhancement of transmission at the developing retinogeniculate synapse. Neuron 1993;10:815–825. [PubMed: 8388224]

Nakamura A, Kobayashi E, Takai T. Exacerbated graft-versus-host disease in Pirb-/- mice. Nature immunology 2004;5:623–629. [PubMed: 15146181]

Penn AA, Riquelme PA, Feller MB, Shatz CJ. Competition in retinogeniculate patterning driven by spontaneous activity. Science (New York, N Y 1998;279:2108–2112.

Prusky GT, West PW, Douglas RM. Behavioral assessment of visual acuity in mice and rats. Vision research 2000;40:2201–2209. [PubMed: 10878281]

Purcell SM, Wray NR, Stone JL, Visscher PM, O'Donovan MC, Sullivan PF, Sklar P. Common polygenic variation contributes to risk of schizophrenia and bipolar disorder. Nature 2009;460:748–752. [PubMed: 19571811]

Robinson L, Bridge H, Riedel G. Visual discrimination learning in the water maze: a novel test for visual acuity. Behav Brain Res 2001;119:77–84. [PubMed: 11164528]

Rossi FM, Pizzorusso T, Porciatti V, Marubio LM, Maffei L, Changeux JP. Requirement of the nicotinic acetylcholine receptor beta 2 subunit for the anatomical and functional development of the visual system. Proc Natl Acad Sci USA 2001;98:6453. [PubMed: 11344259]

Schott E, Bonasio R, Ploegh HL. Elimination in vivo of developing T cells by natural killer cells. The Journal of experimental medicine 2003;198:1213–1224. [PubMed: 14568980]

Shatz CJ, Stryker MP. Prenatal tetrodotoxin infusion blocks segregation of retinogeniculate afferents. Science (New York, N Y 1988;242:87–89.

Shi J, Levinson DF, Duan J, Sanders AR, Zheng Y, Pe'er I, Dudbridge F, Holmans PA, Whittemore AS, Mowry BJ, et al. Common variants on chromosome 6p22.1 are associated with schizophrenia. Nature 2009;460:753–757. [PubMed: 19571809]

Sretavan DW, Shatz CJ, Stryker MP. Modification of retinal ganglion cell axon morphology by prenatal infusion of tetrodotoxin. Nature 1988;336:468–471. [PubMed: 2461517]

Stefansson H, Ophoff RA, Steinberg S, Andreassen OA, Cichon S, Rujescu D, Werge T, Pietilainen OP, Mors O, Mortensen PB, et al. Common variants conferring risk of schizophrenia. Nature 2009;460:744–747. [PubMed: 19571808]

Stellwagen D, Shatz CJ. An instructive role for retinal waves in the development of retinogeniculate connectivity. Neuron 2002;33:357–367. [PubMed: 11832224]

Stevens B, Allen NJ, Vazquez LE, Howell GR, Christopherson KS, Nouri N, Micheva KD, Mehalow AK, Huberman AD, Stafford B, et al. The classical complement cascade mediates CNS synapse elimination. Cell 2007;131:1164–1178. [PubMed: 18083105]

Syken J, Grandpre T, Kanold PO, Shatz CJ. PirB restricts ocular-dominance plasticity in visual cortex. Science (New York, N Y 2006;313:1795–1800.

Tagawa Y, Kanold PO, Majdan M, Shatz CJ. Multiple periods of functional ocular dominance plasticity in mouse visual cortex. Nature neuroscience 2005;8:380–388.

Takai T. Paired immunoglobulin-like receptors and their MHC class I recognition. Immunology 2005;115:433–440. [PubMed: 16011512]

Torborg CL, Feller MB. Unbiased analysis of bulk axonal segregation patterns. Journal of neuroscience methods 2004;135:17–26. [PubMed: 15020085]

van Steensel B, van Binnendijk EP, Hornsby CD, van der Voort HT, Krozowski ZS, de Kloet ER, van Driel R. Partial colocalization of glucocorticoid and mineralocorticoid receptors in discrete compartments in nuclei of rat hippocampus neurons. J Cell Sci 1996;109(Pt 4):787–792. [PubMed: 8718670]

Zinkernagel RM, Doherty PC. MHC-restricted cytotoxic T cells: studies on the biological role of polymorphic major transplantation antigens determining T-cell restriction-specificity, function, and responsiveness. Advances in immunology 1979;27:51–177. [PubMed: 92183]

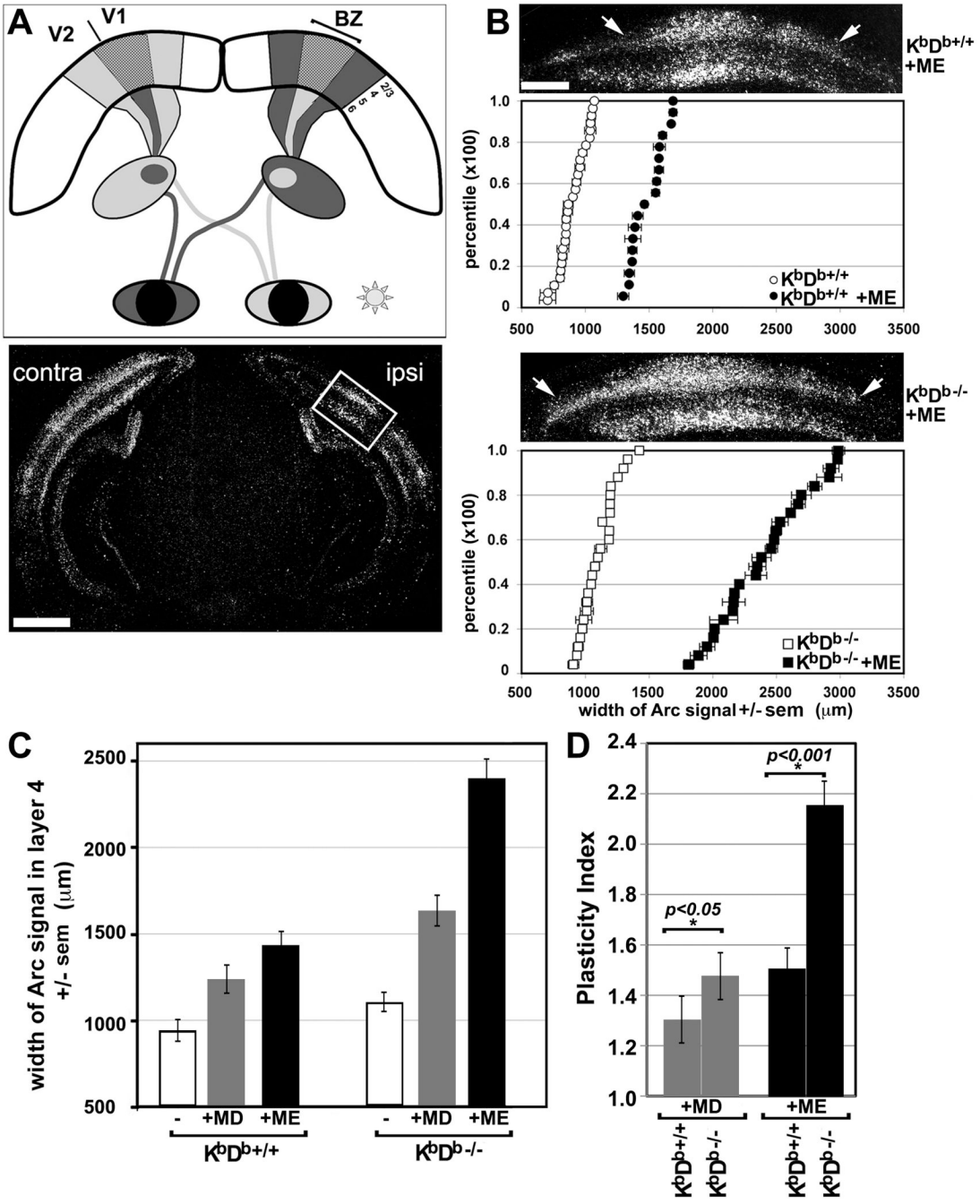

Figure 1. Enhanced ocular dominance plasticity in visual cortex of $K^bD^{b-/-}$ mutant mice

(A) Schematic of mouse visual system. Binocular zone (BZ), located between primary (V1) and secondary (V2) visual cortex, receives input from both eyes. Arc mRNA induction was used to map cortical neurons driven by stimulation of one eye (Experimental procedures and (Tagawa et al., 2005)). Below: darkfield autoradiograph of *Arc* in situ hybridization in a coronal section from a P34 WT ($K^bD^{b+/+}$) mouse; 30 minutes of visual stimulation upregulates *Arc* mRNA in neurons of layers 2-4 and 6 of visual cortex (layer 5 neurons only express very low levels of Arc mRNA). Box indicates region of Arc mRNA upregulation driven by ipsilateral eye stimulation within the BZ; broad induction of Arc mRNA is present throughout V1 and V2 contralateral to the stimulated eye, Scale = 900μm. **(B)** Ipsilateral eye representation in

cortex expands more in $K^bD^{b-/-}$ than in WT ($K^bD^{b+/+}$) mice following monocular enucleation (ME) during the critical period (P22-31). Top: In situ hybridization for Arc mRNA in $K^bD^{b+/+}$ (upper) and $K^bD^{b-/-}$ (lower) visual cortex ipsilateral to the remaining eye; arrows indicate borders of signal in layer 4. Below: cumulative histograms of mean width of Arc induction in layer 4 ± sem for $K^bD^{b+/+}$ (upper) and $K^bD^{b-/-}$ (lower) mice reared with normal vision (open symbols) or mice that received ME (filled symbols). Note increased width of Arc induction following ME in both genotypes. ($K^bD^{b+/+}$+ME: 1426.3 ± 89.7 μm, n = 18 mice vs. $K^bD^{b+/+}$ normal vision: 945 ± 58.3 μm, n = 2 8 mice; $P < 0.05$; $K^bD^{b-/-}$+ME: 2404.6 ± 105.1 μm, n = 25 mice; $P = 0.0017$). Note also that width of Arc induction in $K^bD^{b-/-}$ mutant mice reared with normal visual experience (open squares) is slightly larger than that of normally-reared $K^bD^{b+/+}$ mice (open circles): $K^bD^{b-/-}$: 1111 ± 50.8 μm, n = 25 mice; $K^bD^{b+/+}$: 945 ± 58.3 μm n = 2 8 mice. Each symbol represents the average of several scanned sections from a single animal ± sem. Scale = 400μm. **(C)** Average width of Arc induction in layer 4 for normally reared $K^bD^{b+/+}$ or $K^bD^{b-/-}$ mice (open bar) vs. mice receiving monocular visual deprivation from P25-34 (MD: gray bar, n = 7) or from P22-31 (ME: black bar, n = 25). **(D)** Plasticity Index (see text) reveals greater OD plasticity in $K^bD^{b-/-}$ than in $K^bD^{b+/+}$ visual cortex by MD and ME, (*) statistical significance determined by one-way ANOVA. Error bars = standard error of mean (sem) in **B** and **C**, and root mean square error (RMSE) in D.

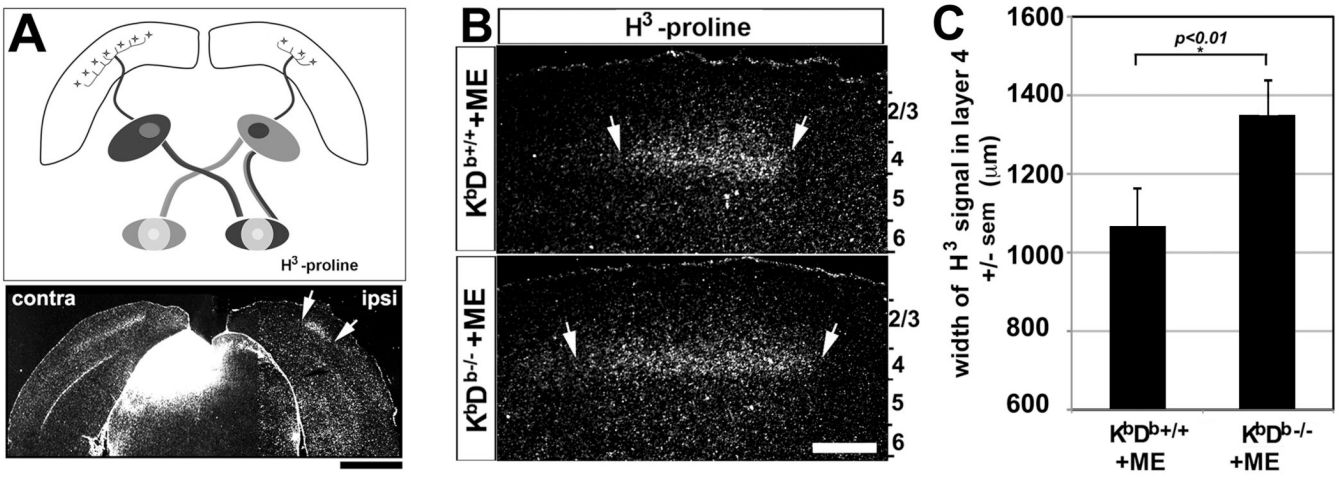

Figure 2. Enhanced thalamocortical plasticity in $K^bD^{b-/-}$ mutant mice

(A) Schematic of connections in mouse visual system: thalamocortical axon terminals innervate layer 4 of cortex. Below, transneuronal transport of H^3–proline following intraocular injection reveals (age P34; Experimental procedures) a broad contralateral signal (left), and smaller ipsilateral patch (right) in layer 4. Scale=1500μm. **(B)** Higher magnification of representative sections from $K^bD^{b+/+}$ (top) and $K^bD^{b-/-}$ (bottom) mice. Arrows indicate measurement borders used. Scale = 450μm. **(C)** Population averages for width ± sem of layer 4 label for each genotype after ME. $P<0.05$; (Mann-Whitney *U* test).

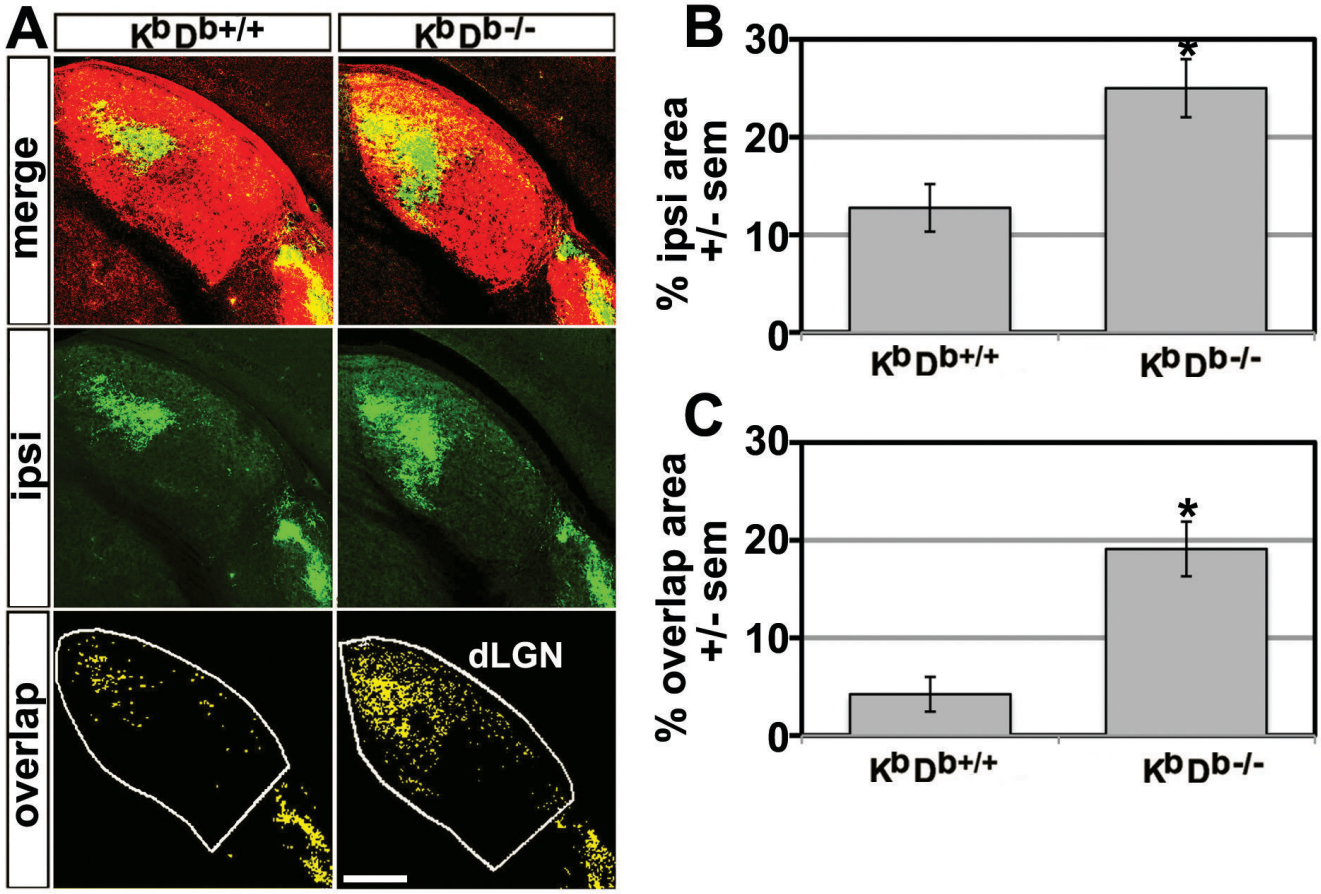

Figure 3. Incomplete segregation of RGC inputs to dLGN in $K^bD^{b-/-}$ mutant mice

(A) RGC projections labeled by intraocular injections of CTB AF594 (red) into the contralateral (contra) eye and CTB AF488 (green) into the ipsilateral (ipsi) eye. Top: Merged fluorescent micrographs of dLGN from $K^bD^{b+/+}$ and $K^bD^{b-/-}$ mice at P34. Middle (green pixels): ipsilateral eye projection pattern (intensity threshold = 60% of maximum). Bottom (yellow pixels): overlapping pixels from ipsilateral and contralateral eye projections each at an intensity threshold 60% of maximum (Figure S3 and Experimental procedures). Note ectopic patches of ipsilateral eye projections not eliminated during development in $K^bD^{b-/-}$ mice. Scale = 150μm. **(B, C)** Mean % of dLGN area ± sem of ipsilateral eye projection and mean overlapping pixels in both channels. More ipsilateral territory as well as overlapping pixels are present in mutant dLGN: $K^bD^{b+/+}$ = 5 mice, $K^bD^{b-/-}$ = 5 mice, $P< 0.05$ (two-tailed *t*-test).

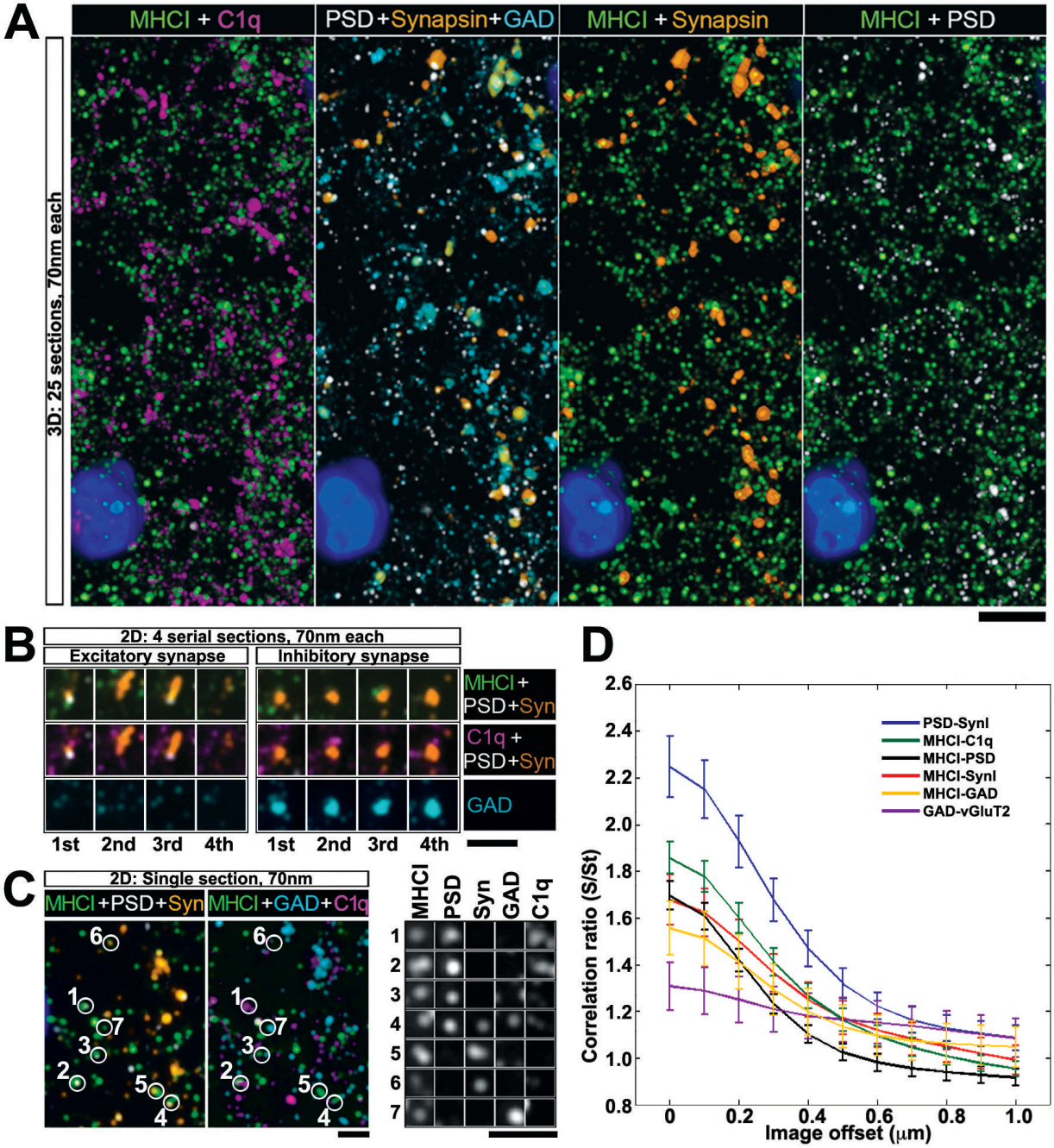

Figure 4. MHCI localization in relation to synaptic proteins during period of retinogeniculate refinement

(A) AT micrographs reconstructed from 25 serial ultrathin sections (each 70nm thick) of P7 LGN showing MHCI immunostaining (green) in relation to known synaptic markers (Syn=synapsin (orange), PSD=postsynaptic density-95 (white), GAD=glutamic acid decarboxylase 65/67 (cyan)), as well as to C1q=complement protein C1q (magenta). DAPI stain of nuclei, blue. Scale = 5μm. **(B)** Four serial sections of 2 different synapsin positive puncta: Left example is characteristic of an excitatory synapse (close apposition of presynaptic marker synapsin with postsynaptic excitatory synapse marker PSD-95); Right example is characteristic of an inhibitory synapse (overlap of synapsin with GAD and absence of PSD-95).

MHCI and C1q are closely associated with both types of synapses. **(C)** Single ultrathin section, showing colocalization between MHCI puncta and PSD, Synapsin, GAD and C1q. Bottom right, zoomed in view of puncta numbered on left, showing immunofluoresence signal in separate channels, Scale = 2μm. Note colocalization of signal for MHCI, PSD and C1q at puncta #1 and 2. **(D)** Cross correlations showing pairwise comparisons of degree of spatial overlap between puncta immunostained for the various markers (Experimental procedures and Figure S4 online). Synapsin vs. PSD95 shows strongest correlation, and GAD vs. vGluT2 the weakest. MHCI is more correlated with C1q than with other markers. Si/St = Cr, the correlation ratio between two channels as a multiple of their baseline correlation. Cr = 1 indicates no correlation, Cr $\gg$ 1 indicates high correlation, Cr < 1 indicates negative correlation.